Z. Phys. C 62, 329–336 (1994)

ZEITSCHRIFT FÜR PHYSIK C

Single diffractive hadron–nucleus interactions within the dual parton model

J. Ranft[1], S. Roesler[2,★]

[1] INFN, Sezione di Milano, Via Celoria 16, I-20133 Milano, Italy
[2] CERN/TIS-RP, CH-1211 Genève 23, Switzerland

Received 1 November 1993

Abstract. Single diffractive hadron-nucleus interactions are studied within the framework of the dual parton model. Introducing a diffractive component into the Monte-Carlo event generator DTUNUC we investigate particle production and the dependence of the diffractive cross section on the atomic number of the target nucleus. A comparison of the numerical results with recent experimental data is presented. We furthermore introduce hadronic cross section fluctuations and discuss their influence on diffractive proton-nucleus cross sections.

1 Introduction

The dual parton model (DPM) (a recent review is given in [1]), a particular realization of the Reggeon field-theory, describes all aspects of soft hadronic reactions in all kinds of high energy collisions. Using the Regge behaviour of parton structure functions, chain-fragmentation models, and the Glauber multiple scattering theory it gives a complete description of hadronic multiparticle production. It has been successfully applied to hadron-hadron, hadron-nucleus and heavy ion collisions.

Early descriptions of diffractive processes within the DPM are due to Innocente et al. [2] and Ranft [3]. The two-component DPM [4–6] connects fundamental ideas of the dual topological unitarization (DTU) scheme [7] with perturbative QCD. It provides a systematic description of diffractive hadron-hadron interactions [8]. There are two components of single diffractive processes: (i) a high mass component represented by the triple-Pomeron graph (high mass single diffraction, HMSD) and (ii) low mass single diffractively excited states (low mass single diffraction, LMSD), described using a two channel eikonal model. A detailed description of single diffractive processes in hadron-hadron collisions within this model and comparisons to data were given recently by Roesler et al. [8].

Using Monte Carlo realizations of the DPM it is possible to test the predictions given by the model comparing them to experimental data. Single diffractive hadron-hadron interactions have been implemented [8] into the DTUJET event generator [5, 6, 9, 10] describing particle production in hadron-hadron collisions within the two-component DPM. The calculated single diffractive cross-sections were in good agreement with experimental data up to collider energies [8].

The Monte Carlo event generator DTUNUC [11–13] has been constructed to study hadron-nucleus and nucleus-nucleus collisions within the DPM. We will implement a diffractive component in DTUNUC to study diffractive hardon-nucleus interactions in the present paper.

Hadron-nucleus diffraction can be characterized as a noncoherent process based on interactions of the projectile hardon with single nucleons of the target nucleus and as the coherent diffraction of the projectile on the nucleus as a whole. Whereas the coherent process has been discussed recently by Frankfurt et al. [14] we are going to study here only the noncoherent diffraction within the DPM.

We present an implementation of incoherent diffractive hadron-nucleus interactions

$$h+A\rightarrow h+A^*$$

and

$$h+A\rightarrow h^*+A$$

into DTUNUC and we compare the results to data on diffractive excitation of the target nuclei (Be, Al, W) in collisions with 450 GeV/c protons measured by the HELIOS-Collaboration [15]. These are the only data on diffractive hadron-nucleus interactions known to us at present.

In Sect. 2 we summarize diffractive hadron-hadron collisions within the two-component DPM and present the implementation of diffractive hadron-nucleus processes within the DPM. In Sect. 3 we calculate single diffractive hadron-nucleus cross sections and compare the

★ *Present address*: University of Siegen, D-57012 Siegen, Germany

model to data. In Sect. 4 we discuss the influence of cross section fluctuations as suggested by Blättel et al. [16] on noncoherent single diffractive hadron-nucleus cross sections. A summary is given in Sect. 5.

2 Single diffraction in the DPM

2.1 Diffractive processes in hadron-hadron interactions

High mass single diffractive hadron-hadron collisions as described in the two-component DPM [6, 8] are represented by the triple-Pomeron graph. A cut triple-Pomeron (TP) graph corresponds to the two chain system shown in Fig. 1. The chains are stretched between a $q\bar{q}$-pair of the Pomeron emitted at the upper vertex and the valence constituents of the excited hadron. Applying Regge-theory it is possible to calculate the differential cross section in the triple-Regge limes, i.e. for $s\to\infty$, $M_D^2\to\infty$, $s/M_D^2\to\infty$, M_D being the mass of the diffractively excited system and $\sqrt{s}$ the c.m. energy

$$\frac{d^2\sigma_{\mathrm{TP}}(s,t)}{dt\,dM_D^2}=\frac{G_{\mathrm{TP}}(t)}{4\pi s_0 M_D^2}\left(\frac{s}{M_D^2}\right)^{2\alpha'_P(0)t}=\frac{G_{\mathrm{TP}}(0)}{4\pi s_0 M_D^2}e^{B_{\mathrm{TP}}(s)t}. \quad (1)$$

All couplings and signature factors have been incorporated into $G_{\mathrm{TP}}(t)=G_{\mathrm{TP}}(0)e^{B^0_{\mathrm{TP}}t}$. $\alpha_P(t)=1+\alpha'_P(0)t$ is the Pomeron trajectory. The scale factor s_0 is chosen to be 1 GeV^2. One obtains a slope decreasing with M_D

$$B_{\mathrm{TP}}(s)=B^0_{\mathrm{TP}}+2\alpha'_P(0)\ln\left(\frac{s}{M_D^2}\right), \quad (2)$$

and the dominating $1/M_D^2$-as well as the exponential t-behaviour of the differential diffractive cross section as confirmed by numerous measurements [17, 18]. The triple-Pomeron cross section can be calculated integrating (1) over t and over M_D^2 from a lower $M_D^{\min}$-cut, determined by our subdivision into LMSD and HMSD, up to $x_D^{\max}s$. The upper cut $x_D^{\max}$ is fixed by the coherence condition [18]

$$\frac{M_D^2}{s}\leq(m_p R)^{-1}=x_D^{\max};\quad R\simeq m_\pi^{-1} \quad (3)$$

where m_p is the proton mass and R the interaction radius.

In order to compute the relative strengths of the various multichain diagrams appearing in the DPM topological expansion their correspondence to Pomeron exchange diagrams in a perturbative Regge approach (we consider the lowest order in the triple-Pomeron coupling, which is assumed to be small) is used. A description of the generalized eikonal model applied to satisfy s-channel unitarity can be found in [1, 6]. Following this formalism we obtain the high mass single diffractive cross section

$$\sigma_{\mathrm{HMSD}}(s)=4\pi\int_0^\infty b\,db\,(e^{\chi_{\mathrm{TP}}(b,s)}-1)\,e^{-2\chi(b,s)} \quad (4)$$

with the eikonal functions $\chi_i(b,s)\,(i=s,\mathrm{TP},L,h)$ and $\chi=\chi_s-\chi_{\mathrm{TP}}-\chi_L+\chi_h$ defined by

$$\chi_i(b,s)=\frac{\sigma_i(s)}{8\pi B_i}e^{-b^2/4B_i},\quad \sigma_i(s)=2\int d^2b\,\chi_i(b,s). \quad (5)$$

We refer to [6] for the definitions of the input cross sections $\sigma_i(s)$ and the eikonal functions of soft (s) processes (corresponding to a single Pomeron exchange), of contributions of graphs containing a Pomeron loop (L), and hard (h) processes described applying lowest order perturbative QCD.

In order to ensure the consistency of this approach, i.e. to avoid a large triple-Pomeron coupling, a low mass single diffractive component has been introduced via a two-channel eikonal model [6]. Diffractively excited states with low masses corresponding to this LMSD component are treated by the excitation of one of the hadrons to intermediate resonances or continuum states with the same quantum numbers as the original hadron. The chain-system which we use for this component [8] is shown in Fig. 2.

2.2 Diffractive scattering of hadrons on nuclei

DTUNUC starts from an impulse approximation for the interacting target nucleus – i.e. with a frozen discrete spatial distribution of nucleons sampled from standard density distributions [19]. The primary interaction of the incident high-energy projectile proceeds via totally n elementary collisions between the projectile and n nucleons from the target nucleus. Actual numbers n are sampled on the basis of Glauber's multiple scattering formalism using the Monte Carlo algorithm of [19]. Note that the projectile hadron may undergo several interactions. Particle production in each elementary collision is described by the fragmentation of two color-neutral parton-parton chains. Those chains are constructed from the valence

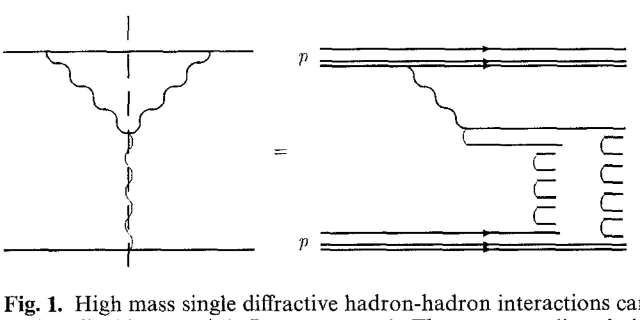

Fig. 1. High mass single diffractive hadron-hadron interactions can be described by the triple-Pomeron graph. The corresponding chain system is shown for proton-proton interactions

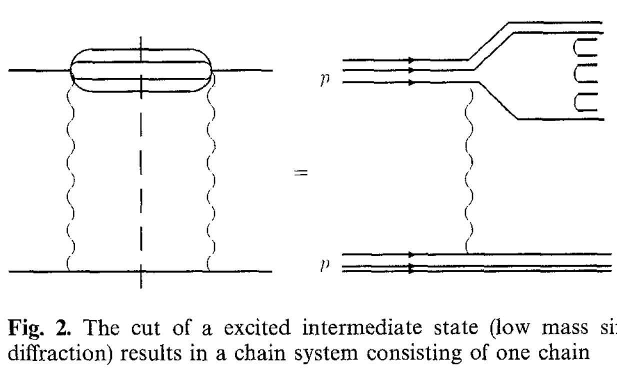

Fig. 2. The cut of a excited intermediate state (low mass single diffraction) results in a chain system consisting of one chain

quark systems or – in the case of repeated scatterings of single hadrons – from sea-$q\bar{q}$ pairs and sea-qq-$\bar{q}\bar{q}$ pairs of the interacting hadrons.

In DTUNUC, intended for low energy applications, we neglect multiple-Pomeron processes in each individual hadron-nucleon collision, because the contributions from multiple strings to single particle densities can be neglected at low energies. This is due to the small average invariant masses of $q\bar{q}$-strings at these energies. Therefore each hadron-nucleon interaction can be approximately described by two chains produced. Considering a configuration with n struck nucleons of the nucleus the chains are stretched between n valence quarks and n valence diquarks of the n target nucleons and the valence and sea constituents of the projectile hadron. The $2n$ chains contribute to the inclusive spectrum of the collision as follows [1]

$$\frac{\mathrm{d}N^{pA}}{\mathrm{d}y}=\frac{1}{\sigma_{pA}}\sum_{n=1}^{A}\sigma_n^{pA}\big[N_n^{qq_v^p-q_v^A}(y)+N_n^{q_v^p-qq_v^A}(y)$$
$$+(n-1)\big(N_n^{q_s^p-qq_v^A}(y)+N_n^{\bar{q}_s^p-q_v^A}(y)\big)\big]. \qquad (6)$$

σ_n^{pA} is the cross section for n inelastic collisions and $\sigma_{pA}=\sum_{n=1}^{A}\sigma_n^{pA}$.

Single diffractive hadron-nucleus interactions as introduced into DTUNUC are treated as Glauber processes involving one single target nucleon only. Most of these are peripheral processes. We assume, that the fractions $\sigma_{sd}^{hn}/\sigma_{\mathrm{inel}}^{hn}$ of these collisions are diffractive. The inelastic cross sections $\sigma_{\mathrm{inel}}^{hn}$ are taken from fits to measured cross sections given in [20] and predictions obtained from the two-component DPM for $p\bar{p}$-collisions at higher energies [10]. The values of hadron-nucleon single diffractive cross sections σ_{sd}^{hn} are obtained from our model [8]. The peripheral character of diffractive proton-nucleus interactions is also supported by experimental observations of the HELIOS-Collaboration [15] emphasizing that the measured dependence of the diffractive cross section on the nuclear mass behaves like

$$\sigma_{sd}=\sigma_0 A^{\alpha}; \quad \sigma_0=(3.8\pm0.3)\,\mathrm{mb}; \quad \alpha=0.35\pm0.02. \qquad (7)$$

In order to compare the predictions given by the model with the data [15] we count only such diffractive interactions in which the projectile hadron remains intact and the involved target nucleon is excited diffractively. The treatment of the chains fragmenting into the diffractive final state is identically to the one described in [8] for hadron-hadron collisions. We again fix the kinematical situation sampling the invariant mass M_D of the system and the momentum transfer t in the hadron-nucleus collision. We determine M_D by choosing the x_D-value defined by the Feynman-x_F variable $x_F=(p'_{h\parallel}/p_h)_{\mathrm{cms}}=1-x_D=1-M_D^2/s$. This is valid in a good approximation at the energies considered. This selection is also limited by the coherence condition (3). The flavors of the $q\bar{q}$-pair of the Pomeron emitted at the upper vertex (see Fig. 1) are chosen from an $SU(3)$-symmetric sea of $q\bar{q}$-pairs as applied for nondiffractive chains [13]. The fragmentation of the individual strings can be handled by BAMJET [21] or optionally by JETSET 7.3 [22]. The results presented in the following section have been obtained using the JETSET fragmentation model with the parameters $b=0.15$ and $\sigma=0.85$ for strings representing high mass and low mass single diffractive interactions. This fragmentation is followed by a formation zone suppressed intranuclear cascade [11, 23]. The produced secondaries are followed along straight trajectories and may induce intranuclear cascade processes if they reach the end of their formation zone inside the target nucleus.

3 Comparison of model predictions with data

3.1 Single diffractive cross sections

The single diffractive cross sections for proton-nucleus interactions presented in this section are obtained on the basis of the Glauber cross sections calculated in DTUNUC taking the fraction of events with only one target nucleon involved into consideration. The results are plotted in Fig. 3 (dots; see also Table 1) for eight different target nuclei together with measured values of p-Be, p-Al

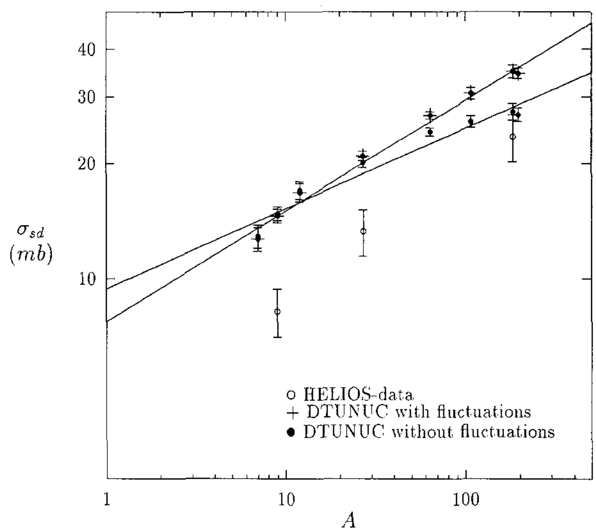

Fig. 3. Single diffractive cross sections calculated without cross section fluctuations (filled dots) and with cross section fluctuations (crosses) for different diffractive proton-nucleus interactions compared with data on Be-, Al- and W-diffraction. The errorbars of the measurements indicate systematic errors [15]. The straight lines correspond to fits to the values calculated with the model

Table 1. Single diffractive proton-nucleus cross sections at 450 GeV/c calculated without cross section fluctuations as well as taken them into account compared to the only data [15] which are available at present

	σ_{sd} (mb) (without fluct.)	σ_{sd} (mb) (with fluct.)	$\sigma_{sd}^{\mathrm{exp}}$ (mb)
p-Li	12.9 ± 0.9	12.7 ± 0.9	
p-Be	14.8 ± 0.6	14.6 ± 0.6	8.21 ± 1.18
p-C	17.0 ± 0.9	16.8 ± 0.9	
p-Al	20.1 ± 0.6	20.9 ± 0.6	13.29 ± 1.84
p-Cu	24.2 ± 0.6	26.8 ± 0.6	
p-Ag	25.8 ± 0.9	30.6 ± 1.1	
p-W	27.4 ± 1.4	34.9 ± 1.4	23.52 ± 3.36
p-Au	26.9 ± 1.1	34.5 ± 1.1	

and p-W single diffractive cross sections [15]. In order to estimate the error within the calculated values we used different initializations of random numbers. The error bars represent the standard deviations. The calculated values are higher than the experimental ones except for p-W interactions where the predicted single diffractive cross section agrees with the measured value within the error. We have assumed, that single diffractive cross sections of interactions where the target nucleon decays diffractively are equal to the ones of those collisions where the projectile hadron decays diffractively within the nucleus. However, there is no experimental evidence supporting this assumption known to us at present. We also show the parameters of a A^{α}-parameterization of our calculated cross sections in Table 2 (column: without fluctuations). The errors are obtained from the ones of the cross sections. We note, that α corresponding to the calculated cross sections is obtained smaller than expected for peripheral collisions.

Table 2. Parameters obtained fitting single diffractive cross sections calculated with and without cross section fluctuations to the parameter representation $\sigma_{sd}=\sigma_0 A^{\alpha}$. They are compared to the parameters given in [15]

	σ_0 (mb)	α
DTUNUC without fluctuations	9.4 ± 1.3	0.21 ± 0.03
DTUNUC with fluctuations	7.7 ± 1.0	0.29 ± 0.03
experiment	3.8 ± 0.3	0.35 ± 0.02

3.2 Diffractive proton-beryllium, -aluminium and -tungsten interactions

Single diffractive interactions of protons on beryllium, aluminium, and tungsten nuclei at 450 GeV/c were investigated by the HELIOS-Collaboration [15]. It should be noted, that we used the coherence condition $M_D^2/s \leq 0.075$ in agreement with [15] for all distributions presented in this section. Furthermore we took in agreement with [15] only those events into consideration in which the values of the transverse momenta of the deflected projectile proton were within the range $0.1\ \mathrm{GeV/c} \leq p_{\perp} \leq 0.6\ \mathrm{GeV/c}$.

In Fig. 4 we show the differential cross sections $d\sigma_{sd}/dx_F$ depending on $(1-x_F)$ for the three target nuclei

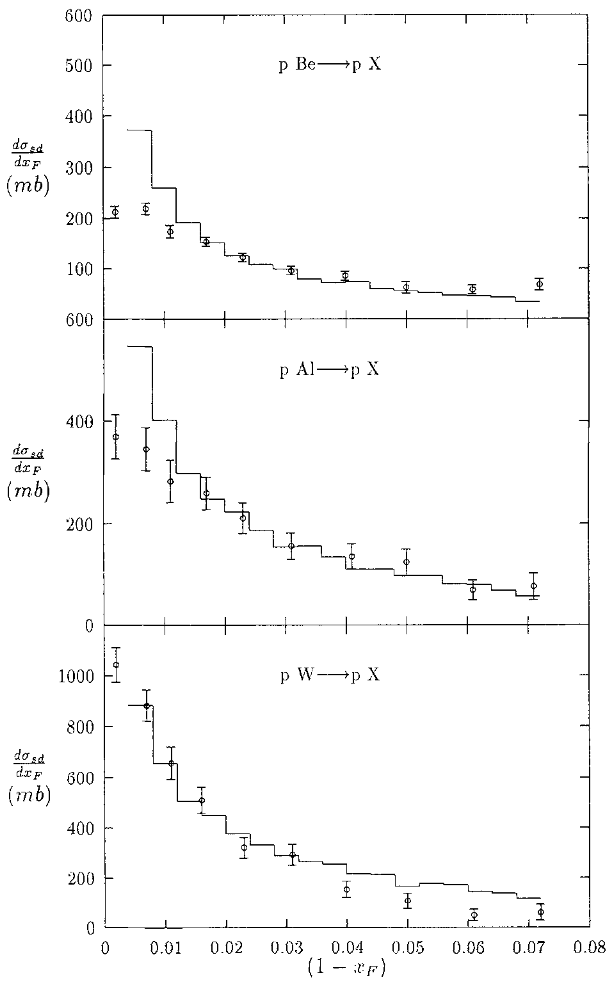

Fig. 4. Comparison of the differential single diffractive cross section $d\sigma_{sd}/dx_F$ depending on the Feynman variable x_F for the nuclear targets beryllium, aluminium and tungsten with experimental data [15]

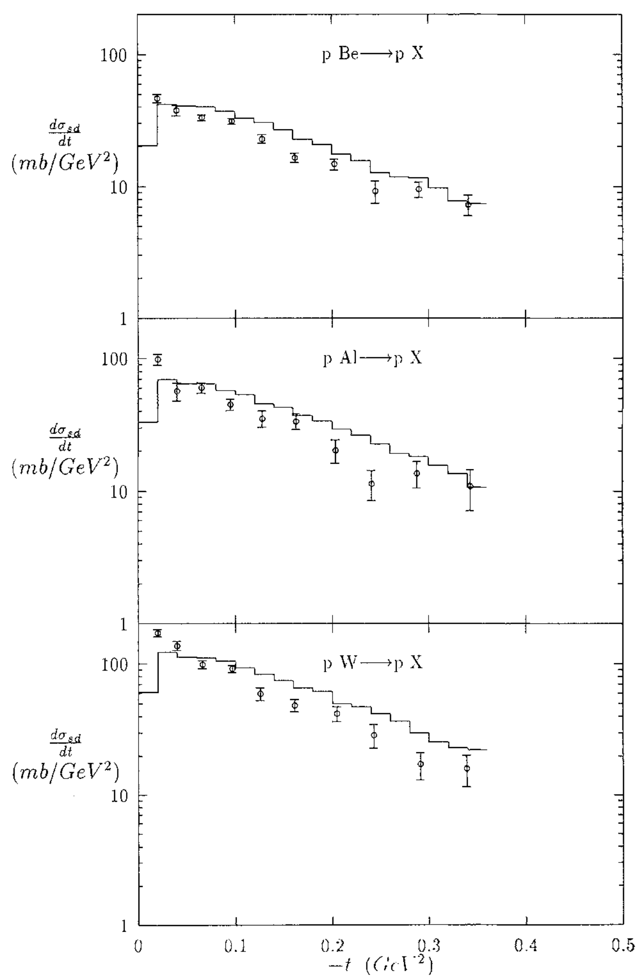

Fig. 5. The differential cross section $d\sigma_{sd}/dt$ as a function of $-t$ for $(M_D^2/s)_{\max}=0.075$ (histogram) is shown together with data of the HELIOS-Collaboration (points) [15]

together with data. In order to compare the shape of the distributions, which clearly show the typical $1/M_D^2$-behavior, they have been normalized to the experimental values of the single diffractive cross sections. The calculated distributions are in a reasonable agreement with the measurements except for p-Be and p-Al interactions, where the model overestimates the data for low diffractive masses.

Integrating $d\sigma_{sd}/dt\,dx_F$ in the mass range mentioned in Sect. 2.1. one obtains the t-distributions $d\sigma_{sd}/dt$ (Fig. 5). Though the measured slopes are slightly steeper than the calculated slopes, the distributions agree with the data within their uncertainties.

In order to investigate the slope parameter for different x_D-bins we show in Fig. 6 and 7 the corresponding t-distributions for p-Be and p-W interactions calculated with the model. The straight lines represent fits to our calculations (thin lines) and the exponential behaviour using measured slopes (thick lines). The calculated slopes are obtained from (2) modified by the Fermi-momenta of the target nucleons, the intranuclear cascade and the cuts applied in agreement with the experiment as mentioned above. The values of the slope parameters are given in

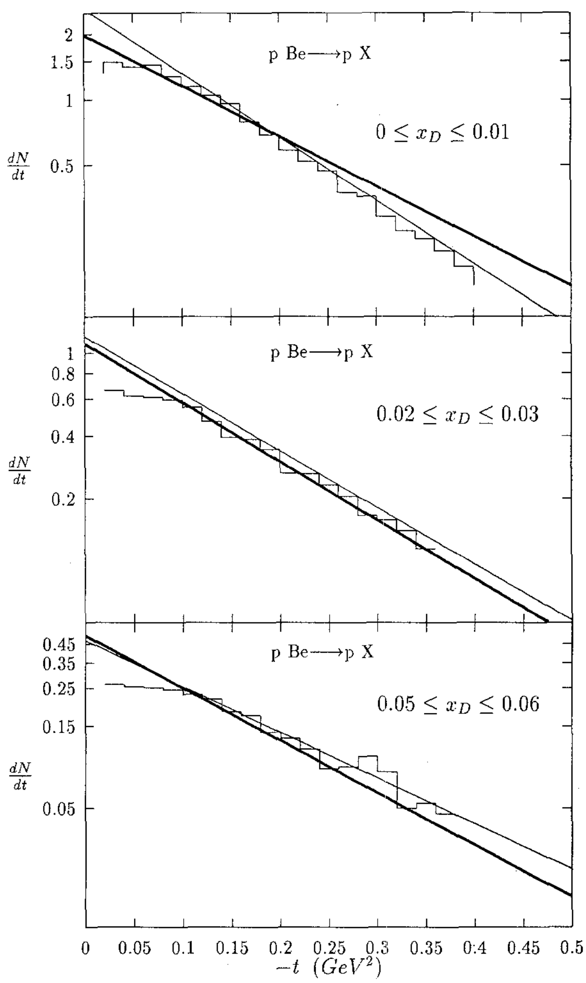

Fig. 6. Slope parameters of the inclusive distribution dN/dt are shown together with data of p-Be diffraction (thick lines). The straight thin lines represent fits to the calculated distributions

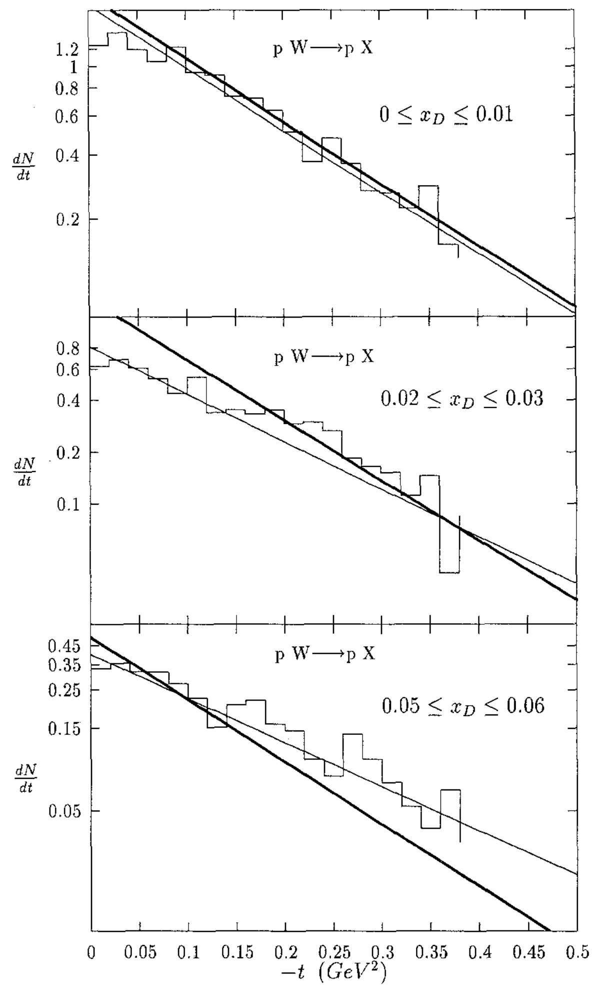

Fig. 7. Slope parameters of the inclusive distribution dN/dt obtained in diffractive p-W interactions are shown for three x_D-bins together with data (thick lines). The straight thin lines represent fits to the calculated distributions

Table 3. As the t-distributions already indicated, the slopes obtained from our model are smaller than the measured values.

The angular distribution of the multiparticle final states (independent of their masses) in diffractive p-Be interactions has been investigated comparing the pseudorapidity distribution to data (Fig. 8). Though it was not clearly mentioned in [15] which particles contributed to the presented distribution, we took all types of particles produced (including gammas from π^0-decays) into consideration. On the basis of this assumption the calculations slightly under-estimate the data at lower pseudorapidities whereas they are overestimated by the model for pseudorapidities above $\eta = 2$.

Figure 9 shows the normalized multiplicity distribution for diffractively decaying Be-nuclei. The agreement between the predictions obtained with the DPM and the data seems to be reasonable.

The mean pseudorapidities of the produced secondaries are shown for Be, Al, and W targets in Fig. 10. The calculated values slightly overestimate the data of p-Be and p-Al interactions at high diffractive masses. The data point at $1-x_F \approx 0.085$ indicates that in contradiction to

Table 3. Calculated slope parameters for different x_D-bins are shown together with measured values [15]

	p-Be $b\,(\mathrm{GeV/c})^{-2}$	p-Be $b^{\exp}\,(\mathrm{GeV/c})^{-2}$	p-W $b\,(\mathrm{GeV/c})^{-2}$	p-W $b^{\exp}\,(\mathrm{GeV/c})^{-2}$
$0 \leq x_D \leq 0.01$	6.7	5.3 ± 0.5	6.5	6.6 ± 0.5
$0.02 \leq x_D \leq 0.03$	6.3	6.5 ± 0.5	6.3	8.0 ± 0.8
$0.05 \leq x_D \leq 0.06$	6.1	7.0 ± 0.5	5.9	8.3 ± 0.7

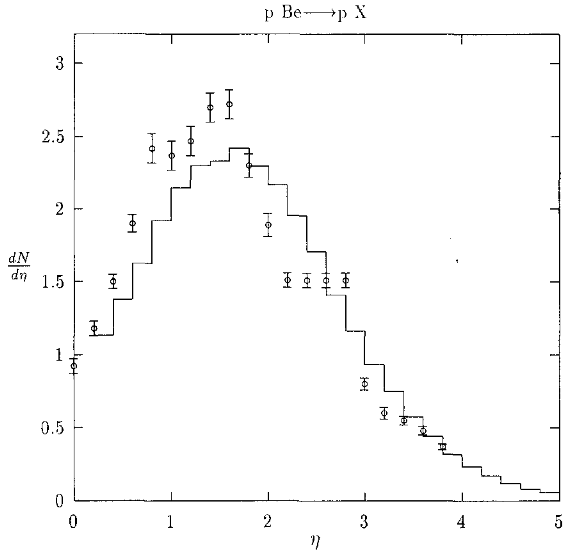

Fig. 8. The pseudorapidity distribution of the multiparticle final state in diffractive p-Be interactions is compared to data [15]

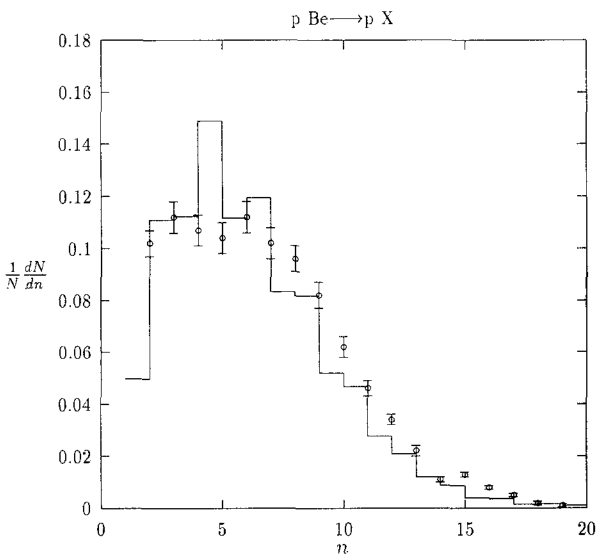

Fig. 9. Multiplicity distribution in diffractive proton-Beryllium interactions. The points correspond to data obtained by the HELIOS collaboration [15]

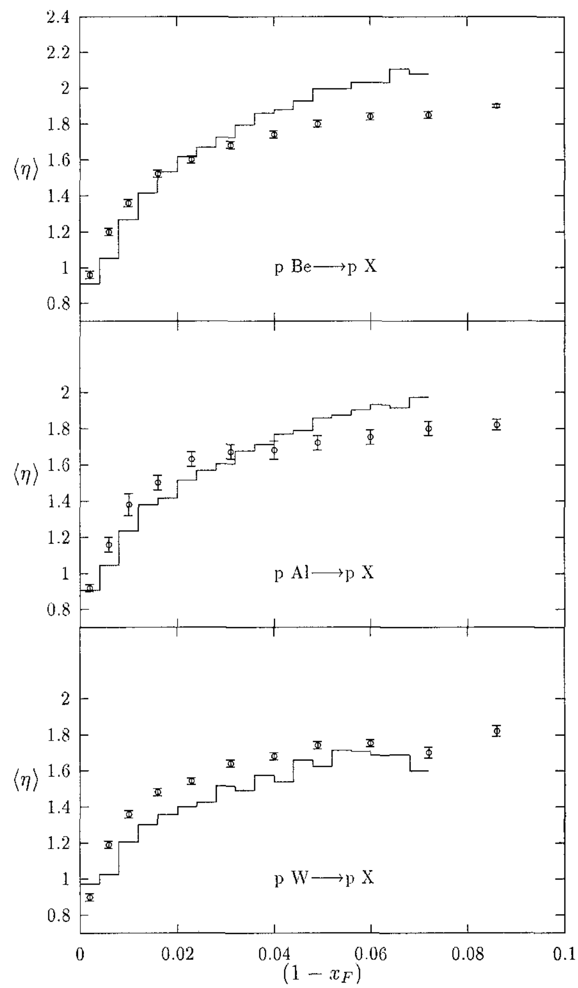

Fig. 10. Mean pseudorapidities for different target nuclei obtained with the model (histogram) are plotted together with data (points) [15]

the coherence condition given in [15] final states with $(1-x_F)>0.075$ has been taken into consideration.

In Fig. 11 the mean transverse momenta of the secondaries are compared to data. They agree well within the experimental uncertainties.

Finally we have investigated the mean multiplicities depending on M_D for all three target nuclei. The comparison is shown in Fig. 12. The calculated values are considerably smaller than the measurements except for small diffractive masses.

4 Influence of cross section fluctuations to single diffractive cross sections

As it has been stressed by Blättel et al. [16, 24] the physics of color transparency and color opacity can be incorporated into the description of nuclear collisions at high energies using the concept of hadronic cross section fluctuations.

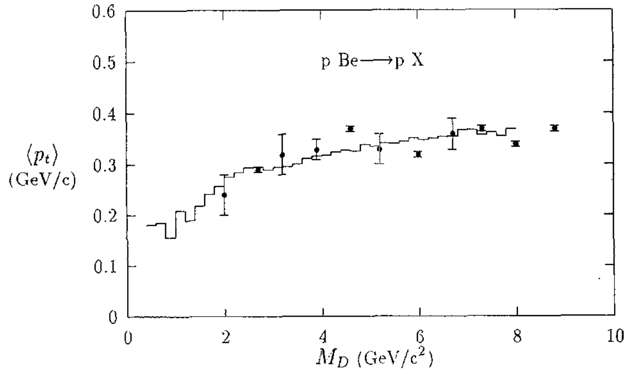

Fig. 11. Average transverse momenta of the produced particles as a function of the diffractive mass M_D shown together with data of the HELIOS-Collaboration [15] for diffraction of beryllium nuclei

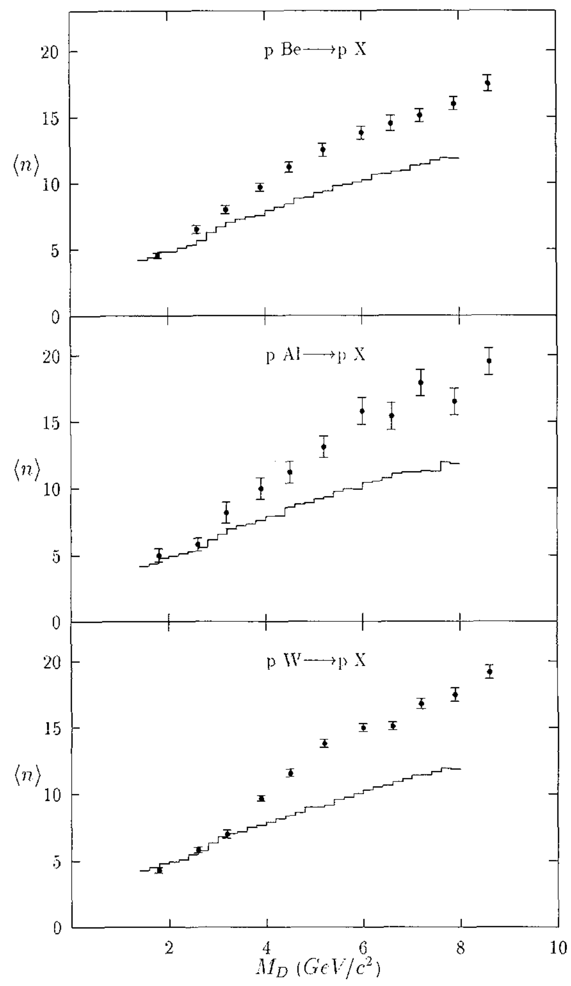

Fig. 12. Average multiplicities of charged and neutral particles depending on the mass of the diffractively produced system M_D are shown for diffractive p-Be, p-Al, and p-W interactions together with data (points) [15]

We have introduced cross section fluctuations into the Glauber framework using the distribution

$$P(\sigma)=N(a,n)\,\frac{\sigma/\sigma_0}{\sigma/\sigma_0+a}\exp\left[-\left(\frac{\sigma-\sigma_0}{\Omega\sigma_0}\right)^n\right] \tag{8}$$

with $\Omega=1.1$, $a=0.1$, $n=6$ and $\sigma_0/\bar{\sigma}=0.893$ as given in [16]. Single diffractive cross sections for different target nuclei calculated taking cross section fluctuations into consideration are shown in Table 1. They are furthermore compared to the values obtained without cross section fluctuations and to data in Fig. 3. Again we have fitted them to the A^α-parametrization and show the results in Table 2. The errors within the calculated values of the cross sections and the parameters have been estimated as mentioned in Sect. 3.1. We now find the α-parameter in agreement with [15] and with the expectations for peripheral collisions.

5 Summary and conclusions

Introducing noncoherent diffractive hadron-nucleus interactions into our Monte-Carlo event generator DTUNUC we have been investigating these processes within the DPM. They are treated as mainly peripheral processes as confirmed by measurements. Our description is therefore based on diffractive interactions of the projectile hadron on a single target nucleon. Taking Fermi-momenta of the target nucleons and the formation zone intranuclear cascades of the diffractively produced secondaries into account we have compared the predictions given by the DPM to data obtained by the HELIOS-Collaboration. They are the only data available at present and can be considered as the results of a first attempt to investigate diffractive dissociation of nuclei systematically.

The single diffractive cross sections calculated with the model overestimate the measured values. This indicates that modifications of the model proposed in this paper have to be introduced as soon as new data confirm the HELIOS measurements [15].

Introducing cross section fluctuations into the Glauber formalism we are able to reproduce the power-law behaviour of a fit to the data.

The detailed comparison of our results on diffractive particle production to data has shown that the measured M_D- and t-dependence of the differential diffractive cross section is well described within the triple-Pomeron regime representing diffractive hadron-nucleon interactions. However there are difficulties to reproduce the average multiplicities and the slopes presented by the HELIOS-Collaboration.

Acknowledgements. One of the authors (J.R.) acknowledges discussions on cross section fluctuations with M. Strikman. We are grateful to our collaborator H.-J. Möhring for writing the DTUNUC-code.

References

1. A. Capella, U. Sukhatme, C.I. Tan, J. Tran Thanh Van: Orsay Preprint, LPTHE 92-38, to be published in Phys. Rep., 1992
2. V. Innocente, A. Capella, A.V. Ramallo, J. Tran Thanh Van: Phys. Lett. 169B (1986) 285
3. J. Ranft: Z. Phys. C33 (1987) 517
4. A. Capella, J. Tran Thanh Van, J. Kwiecinski: Phys. Rev. Lett. 58 (1987) 2015

5. F.W. Bopp, A. Capella, J. Ranft, J. Tran Thanh Van: Z. Phys. C51 (1991) 99
6. P. Aurenche, et al.: Phys. Rev. D45 (1992) 92
7. G.F. Chew, C. Rosenzweig: Nucl. Phys. B104 (1976) 290; C. Hong-Mo, J.E. Paton, T. Sheung Tsun: Nucl. Phys. B86 (1975) 470
8. S. Roesler, R. Engel, J. Ranft: Z. Phys. C59 (1993) 481
9. K. Hahn, J. Ranft: Phys. Rev. D41 (1990) 1463; F.W. Bopp, D. Pertermann, J. Ranft: Z. Phys. C54 (1992) 683
10. R. Engel, F.W. Bopp, D. Pertermann, J. Ranft: Phys. Rev. D46 (1992) 5192
11. H.-J. Möhring, J. Ranft: Z. Phys. C52 (1991) 643
12. I. Kawrakow, H.J. Möhring, J. Ranft: Nucl. Phys. A544 (1992) 471; I. Kawrakow, H.J. Möhring, J. Ranft: Z. Phys. C56 (1992) 115; H.J. Möhring, J. Ranft, A. Capella, J. Tran Thanh Van: Phys. Rev. C47 (1993) 4146; I. Kawrakow, H.J. Möhring, J. Ranft: Phys. Rev. D47 (1993) 3849
13. J. Ranft, A. Capella, J. Tran Thanh Van: Preprint Lund University, LU TP 93-18, 1993
14. L. Frankfurt, G.A. Miller, M. Strikman: Evidence for color fluctuations in hadrons from coherent nuclear diffraction, 1993
15. T. Åkesson et al., HELIOS-Coll.: Z. Phys. C49 (1991) 355
16. B. Blättel et al.: Phys. Rev. D47 (1993) 2761
17. M. Bozzo et al., UA4 Coll.: Phys. Lett. 136B (1984) 217; D. Bernard et al., UA4 Coll.: Phys. Lett. 186B (1987) 227
18. K. Goulianos: Phys. Rep. 101 (1983) 169
19. S.Y. Shmakov, V.V. Uzhinskii, A.M. Zadoroshny: Comput. Phys. Commun. 54 (1989) 125
20. Particle Data Group: Phys. Rev. D45 (1992) 1
21. S. Ritter: Comput. Phys. Commun. 31 (1984) 393
22. T. Sjöstrand: CERN Report CERN-TH.6488/92, 1992
23. J. Ranft: Z. Phys. C43 (1989) 439
24. B. Blättel et al.: Nucl. Phys. A544 (1992) 479